ACS APPLIED MATERIALS & INTERFACES

RESEARCH ARTICLE

www.acsami.org

Simple Electrochemical Deposition of Au Nanoplates from Au(I) Cyanide Complexes and Their Electrocatalytic Activities

Bora Seo, Suhee Choi, and Jongwon Kim*

Department of Chemistry, Chungbuk National University, Cheongju, Chungbuk 361-763, Korea

Supporting Information

ABSTRACT: Nanostructured Au surfaces have unique and attractive properties as functional materials in many fields such as heterogeneous catalysis and electrocatalysis. Electrochemical deposition of Au has received much attention as a simple route for the fabrication of Au surface nanostructures. In this study, we report a simple electrodeposition of Au nanoplate structures from $Au(CN)_2^-$ on Au surfaces in the absence of additives or premodification of electrode surfaces. The shape of the Au nanoplates as well as their surface structures is unique compared to other Au nanostructures electrodeposited from commonly employed $AuCl_4^-$ complexes. The nanoplate Au surfaces exhibit unique electrocatalytic activities for oxygen reduction and glucose oxidation, which originate from the Au(110) and Au(100) facets present on nanoplate surfaces. A simple preparation of well-defined Au nanoplate structures would allow new opportunities in various areas utilizing Au-based substrates through further modification of Au surfaces.

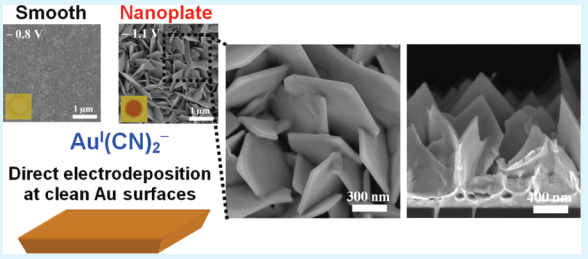

KEYWORDS: electrodeposition, gold cyanide, nanoplate structure, glucose oxidation, oxygen reduction

INTRODUCTION

The fabrication of nanostructured Au surfaces has been the subject of intensive research because such surfaces provide important applications in heterogeneous catalysis, biological labeling, and electrocatalysis. Following recent developments in the synthesis of Au nanoparticles (AuNPs) of various sizes and shapes, as well as in the management of their physical and chemical properties,[1] much attention has been paid to the assemblies of AuNPs on surfaces for constructing hierarchical Au nanostructures to utilize the unique properties of AuNPs. Charged polymers or thiolated molecules were traditionally employed to assemble solution-dispersed AuNPs on surfaces.[2,3] However, the linker molecules or capping agents on AuNPs may affect the surface chemistry of the resultant nanoparticle assemblies, which is ultimately not ideal for many applications, particularly electroanalytical ones.

Electrochemical deposition of Au offers an alternative route for the fabrication of Au surface nanostructures. Ohsaka et al. electrodeposited AuNPs on electrode surfaces, which exhibit unique electrocatalytic activity for oxygen reduction.[4] Since then, numerous efforts have been made to form various Au nanostructures on electrode surfaces by electrodeposition.[5,6] In many cases, electrodeposition of nanostructured Au architectures requires either the premodification of electrode surfaces or the presence of additives. Recently, much attention has been focused on the fabrication of surface nanostructures by simple electrodeposition on a clean surface in the absence of additives or surfactants.[7−10]

Here, we report a simple electrodeposition of Au nanoplate structures on Au surfaces without any surfactants, templates, or premodifications of electrode surfaces. Most of the recent solution-phase synthesis of AuNPs or Au electrodepositions to fabricate nanostructured electrode surfaces employed Au(III) complexes, typically $AuCl_4^-$, whereas the utilization of Au(I) complexes has been rather limited. This is probably due to the low solubility and instability of Au(I) complexes; however, they have recently received much attention as alternative and better precursors than Au(III) complexes for the controllable synthesis of AuNPs by forming Au(I) complexes with proper ligands.[11] In this work, we used a Au(I) cyanide complex, $Au(CN)_2^-$, as a precursor for Au electrodeposition. The Au(I) cyanide complexes are stable in aqueous phase and have historically been used in the microelectronics industries for producing soft and smooth Au deposits.[12,13] We show that $Au(CN)_2^-$ can be used for the electrodeposition of Au to obtain well-defined nanoplate Au structures on Au electrode surfaces under the optimized electrochemical conditions. The morphological variations of Au deposits with different electrodeposition conditions are monitored by scanning electron microscopy (SEM) and the surface structures and electrocatalytic activities of Au nanoplates are examined.

EXPERIMENTAL SECTION

Reagents and Instruments. All solutions were prepared using purified water (Milli-Q, 18.2 MΩ·cm). $KAu(CN)_2$, Na_2CO_3, $Pb(NO_3)_2$,

Received: October 21, 2010
Accepted: December 30, 2010
Published: January 19, 2011

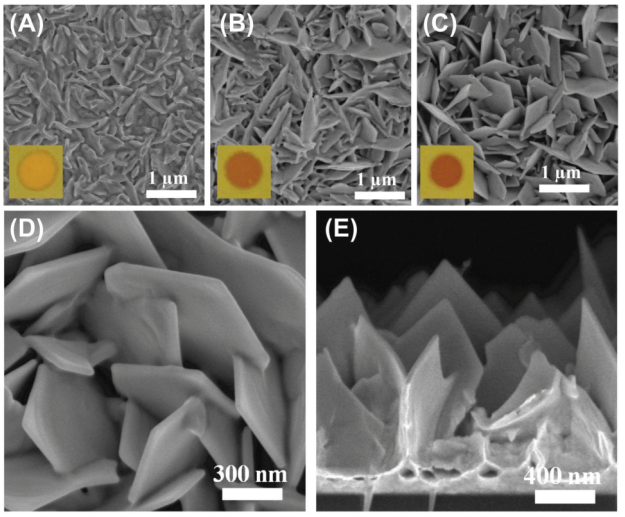

Figure 1. SEM images of Au deposits electrodeposited from a solution containing 15 mM $KAu(CN)_2$ and 0.25 M Na_2CO_3 at (A) −0.9, (B) −1.0, and (C) −1.1 V. Total deposition charges are 0.04 C. (D, E) High-resolution and cross-sectional SEM images of C.

glucose, and all other chemicals were obtained from Aldrich and used as received. Electrochemical measurements were conducted using a CHI 400A (CH Instrument) potentiostat. Pt wire and Ag/AgCl electrodes were used as counter and reference electrodes, respectively. All potentials are reported relative to the Ag/AgCl reference electrode (3 M KCl). Scanning electron microscopy (SEM) characterization was performed using a LEO 1530 Field Emission SEM (Carl Zeiss) with an acceleration voltage of 5 kV. X-ray diffraction (XRD) data were obtained with a D8 Discover with GADDS (Bruker AXS). Rotating disk electrode data were obtained using a Pine Model MSRX rotator.

Electrochemical Deposition. Au films evaporated onto silicon (Au/Si) wafers (KMAC, Korea) were employed as substrates and cleaned for 1 min in a piranha solution (1:3 by volume of 30% H_2O_2 and H_2SO_4, ***Caution:*** *piranha solution reacts violently with most organic materials and must be handled with extreme care*). The cleaned Au substrate was confined in a Viton O-ring with an inner diameter of 2.9 mm and used as a working electrode. Electrodeposition was performed from a solution containing $KAu(CN)_2$ (typically 15 mM; ***Caution:*** *$KAu(CN)_2$ is a toxic material and must be handled with care*) and 0.25 M Na_2CO_3. A constant deposition potential was applied, and the total deposition charge was regulated. A typical condition for the formation of well-defined nanoplate structures was −1.1 V of deposition potential with 0.04 C of deposition charge.

RESULTS AND DISCUSSION

Effect of Deposition Conditions on the Morphology of Au Deposits. Au nanoplate structures are typically electrodeposited on Au surfaces from a solution containing 15 mM $KAu(CN)_2$ and 0.25 M Na_2CO_3 at a constant applied potential of −1.1 V. Figure 1 shows SEM images of Au structures electrodeposited at various deposition potentials. When a deposition potential of −0.8 V was applied, the Au deposits were flat and shiny, almost identical to bare Au surfaces (see Figure S1 in the Supporting Information). Flake-type Au deposits start to form with an applied potential of −0.9 V, and the shape of Au deposits become more defined as more-negative deposition potentials are applied. Well-defined nanoplate structures were obtained at −1.1 V, whereas the application of a more-negative deposition potential (ca. −1.2 V) resulted in the collapse of the nanoplate structures (see Figure S1 in the Supporting Information). Insets in Figure 1 show optical images of the macroscopic surfaces of the Au deposits, where the color of surfaces changes from orange to light brown, indicating that the localized plasmon resonance is different at each nanostructured surface.[7] Illustrated in images D and E in Figure 1 are detailed features of well-defined Au nanoplate structures, where the thickness of the nanoplates is typically ca. 50 nm and the width spans from 500 to 800 nm. A similar Au nanoplate structures have been previously synthesized through liquid-phase reduction from AuNPs attached on indium tin oxide surfaces in the presence of poly-(vinylpyrrolidone) additives.[14,15]

The cross-sectional SEM images reveal more detailed deposition patterns in a vertical direction (see Figure S2 in the Supporting Information). At relatively positive deposition potentials, smooth Au deposits grow initially, followed by the formation of flakes at the end of the deposition process. With more negative potentials, the thickness of smooth Au deposits decreases, and the formation of flake or plate structures begins at earlier stages. At the deposition potential of −1.1 V, well-defined nanoplate structures are achieved, whereas a more-negative deposition potential results in the collapse of the defined structures.

We also examined the effect of the concentration of $Au(CN)_2^-$ on the morphology of the Au deposits (see Figure S3 in the Supporting Information). Lower concentrations of $Au(CN)_2^-$ result in Au deposits with less-defined shapes, whereas higher concentrations of $Au(CN)_2^-$ produce smaller and denser Au nanoflakes interconnected with adjacent ones. Although plate-type Au structures could be obtained with a concentration range of $KAu(CN)_2$ between 10 mM and 30 mM, well-defined nanoplate structures were observed with a $KAu(CN)_2$ concentration of 15 mM. With regard to the effect of supporting electrolytes, we performed electrodepositions from solutions containing 15 mM $KAu(CN)_2$ and 0.25 M Na_2SO_4 either at pH 6.8 (as prepared) or adjusted to 11.6 (same as the pH of a 0.25 M Na_2CO_3 solution). The well-defined nanoplate Au structures were obtained regardless of the supporting electrolytes and the pH of solutions (see Figure S4 in the Supporting Information). These results suggest that the deposition potential with a proper concentration of $KAu(CN)_2$ is critical for the formation of well-defined nanoplate Au structures (vide infra for the effect of electrodeposition potentials), whereas the conditions related to supporting electrolytes such as anionic species and pH do not play significant roles.

With an optimized condition of electrodeposition for Au nanoplate formation, the growth of nanoplates was monitored by varying the total deposition charges (Figure 2). At an early deposition stage, the deposition current quickly decreases and then gradually increases up to 0.02 C. The initial current decay is related to the double-layer charging process, while the subsequent current increase corresponds to the nucleation and growth of the Au deposits.[16] At this stage, flake-shaped Au protrusions are formed on Au surfaces; the deposition current then remains at a constant level, and the nanoplates start to grow. Defined nanoplate shapes with triangular edges start to form with deposition charges of ca. 0.03 C, and the nanoplates then grow anisotropically without a change in thickness. The application of 0.08 C produces a pentagonal nanoplate up to 1 μm in width. Because the deposition charge of 0.04 C is sufficient for the formation of well-defined nanoplates, we elected to apply this deposition charge in subsequent investigations.

Characterization of Nanoplate Au Structures. The Au nanoplate surface was characterized by electrochemical methods.

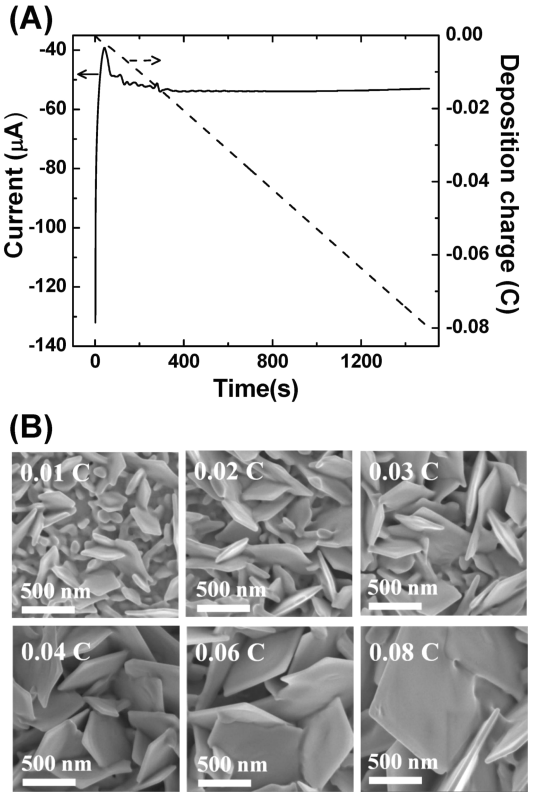

Figure 2. (A) Current and deposition charge vs time curve during electrodeposition in 15 mM $KAu(CN)_2$ + 0.25 M Na_2CO_3 at −1.1 V. (B) SEM images as a function of deposition charge.

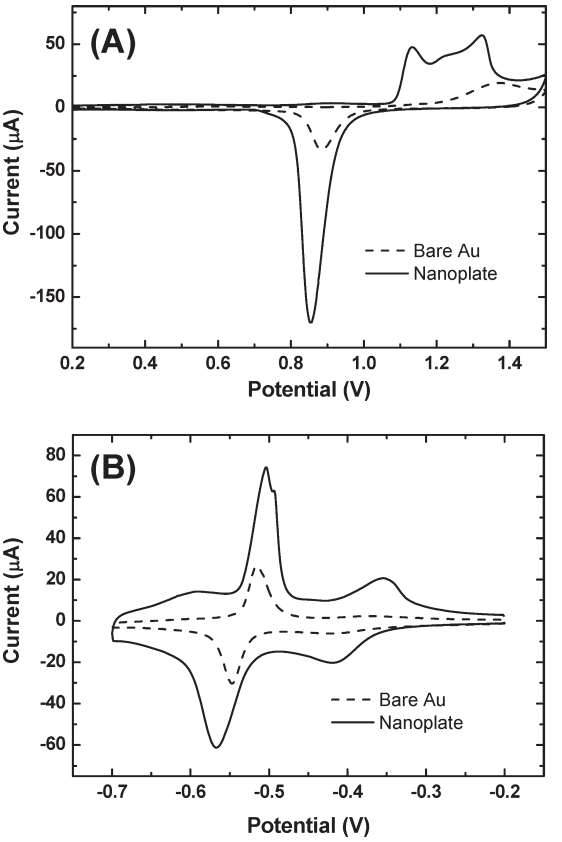

Figure 3. (A) Cyclic voltammograms obtained on bare and nanoplate Au surfaces in 0.1 M H_2SO_4. (B) Pb UPD voltammetric profile of bare and nanoplate Au in 0.1 M NaOH + 10^{-3} M $Pb(NO_3)_2$. Scan rate: 50 mV/s.

Figure 3A shows the cyclic voltammogram of a Au nanoplate electrode in the Au oxide formation and dissolution region, where an increase in the cathodic peak current at 0.85 V indicates that the formation of nanoplate structures results in an increase in the electrochemical surface area (ESA). The ESA of Au deposits estimated by integrating the charge consumed for the reduction of the surface oxide layer[17] gradually increases as increasingly negative deposition potentials are applied from −0.9 V to −1.1 V (see Figure S5 in the Supporting Information). The ESA of the nanoplate electrode electrodeposited at −1.1 V is ca. 4.5 times greater than that of a bare Au surface, and the application of a greater negative potential of −1.2 V resulted in a sharp decrease in the ESA.

Another notable feature from Figure 3A concerns aspects of the surface orientation of Au surfaces in contact with electrolyte solutions. A bare Au surface exhibits a broad anodic peak at around 1.37 V, which is typically found on polycrystalline Au surfaces.[6] Upon the formation of nanoplate Au structures, new anodic peaks develop at 1.14 and 1.32 V. The latter anodic peak is known to originate from the oxide formation of Au at a crystalline facet of (111), while the former peak is observed at Au(110) or Au(100).[18] The surface orientation of nanoplate electrodes was further examined by an underpotential deposition of lead (Pb UPD), during which process the anodic stripping peak potentials can be used as indicators to characterize the surface structure of the electrode.[19,20] Figure 3B shows the UPD curves observed on the nanoplate Au surfaces, where an anodic peak at −0.35 V is clearly visible. This peak can be assigned to the (110) facet of the nanoplate Au surfaces,[20] and is not observed on a bare Au surface. The anodic peaks at around −0.51 V, observed on both the bare and the nanoplate Au surfaces, correspond to the (111) facet on Au surfaces. The larger anodic peak current on Au nanoplate surfaces is due to the increase in ESA of the nanoplate surface compared with that of bare Au surfaces. A shoulder peak is found at approximately −0.49 V, and this potential is close to that observed on the Au(100) crystalline surface.[20,21] An X-ray diffraction (XRD) spectrum of the nanoplate electrode was obtained and subtracted from the background spectrum of an underlying Au substrate (see Figure S6 in the Supporting Information), which also supports the presence of a significant amount of Au(110) and Au(100) crystalline domains on nanoplate Au structures. It is notable that in the XRD data a high-index Au(311) facet is observed, which suggests the presence of atomic steps and kinks on the nanoplate Au structures.[6]

It would be worthy to compare the electrodeposition of Au from $Au(CN)_2^-$ with that from $AuCl_4^-$, which has frequently been used in recent nanoarchitecture formation by electrodeposition. It was reported that electrodeposition of Au from $AuCl_4^-$ on Au electrode surfaces produces Au deposits round in shape, such as rods, spheres, and spikes.[6,7] We also examined the morphology of the Au deposits from $AuCl_4^-$ at various deposition potentials, but plate-type deposits were not observed (see Figure S7 in the Supporting Information). The nanoplate Au structures electrodeposited from $Au(CN)_2^-$ observed in this work are therefore unique in shape compared to Au nanostructures electrodeposited from $AuCl_4^-$. In addition to the difference in morphologies, it is notable that the Au nanoplate structures are relatively rich in (110) or (100) domains, whereas the Au nanostructures electrodeposited from $AuCl_4^-$ are predominantly oriented in

(111) facets. This could be a favorable feature of nanoplate Au structures for electroanalytical applications, because the (110) and (100) facets are electrocatalytically more active than the (111) facet in many electrochemical reactions owing to their high surface energies.[22] It should be noted that the Au nanostructures electrodeposited from $AuCl_4^-$ have been shown to exhibit electrocatalytic activities because of the introduction of surface nanostructures, even though they are dominantly faceted by (111) domains.[6,7]

The Au reduction process from Au(I) cyanide complex, $Au(CN)_2^-$, can occur through the following direct deposition process as follow at high cathodic overpotentials[23−25]

$$Au(CN)_2^- + e^- \rightarrow Au + 2CN^- \quad (1)$$

At low overpotentials, on the other hand, a special chemical-electrochemical mechanism applies, where the complex is first chemically adsorbed on electrode surfaces followed by the electrochemical reduction step[23−26]

$$Au(CN)_2^- \rightarrow Au(CN)_{ad} + CN^- \quad (2)$$

$$Au(CN)_{ad} + e^- \rightarrow Au + CN^- \quad (3)$$

The deposition potential of −1.1 V employed in this work for nanoplate formation corresponds to the low overpotential region (see Figure S8 in the Supporting Information), and thus the latter mechanism (eqs 2 and 3) can be applied. We believe that after the initial formation of flake-shaped Au protrusions, further growth of Au prefers on the edge site of the Au deposits. The edge side of nanoplate Au structures is known to be faced by (110) planes,[27] on which the rate determining reduction step (eq 3)[25] occur more favorably than the plane side, resulting in the anisotropic growth of the nanoplate structures. In addition, it was reported that anisotropic nanostructures such as nanoplates can be synthesized in a solution phase at a slow reduction rate under kinetic controls.[28] Therefore, the deposition potential corresponding to a low overpotential plays an important role for the formation of nanoplate.

Electrocatalytic Activities of Nanoplate Au Structures. The electrocatalytic activity of the nanoplate surface was examined for oxygen reduction and glucose oxidation reactions, which are of prime importance in electrochemical applications of nanostructured electrode surfaces in energy conversion and electroanalysis. Figure 4A compares the cyclic voltammograms obtained on nanoplate and bare Au surfaces in basic media. The cathodic peak potentials for oxygen reduction shift positively on nanoplate surfaces, and the current density also increases compared with that on a bare Au surface, indicating that the nanoplate surfaces are electrocatalytically active for oxygen reduction. Because it is well-known that oxygen reduction is more active at Au(100) and Au(110) than at Au(111) in basic media,[29] the electrocatalytic activity at nanoplate surfaces can be attributed to the introduction of (100) and (110) facets on nanoplate Au surfaces. Specifically, the Au(100) is known to be electrocatalytically active toward the four-electron reduction of oxygen to water in basic media. To examine the reduction mechanism of oxygen on the nanoplate electrode surface, we performed rotating disk electrode (RDE) experiments. Figure 4B shows the Koutecky−Levich plots obtained from RDE measurements, where the number of electrons associated with the oxygen reduction is four on the Au nanoplate electrode, while that found on a bare Au surface is two. This result clearly indicates that the

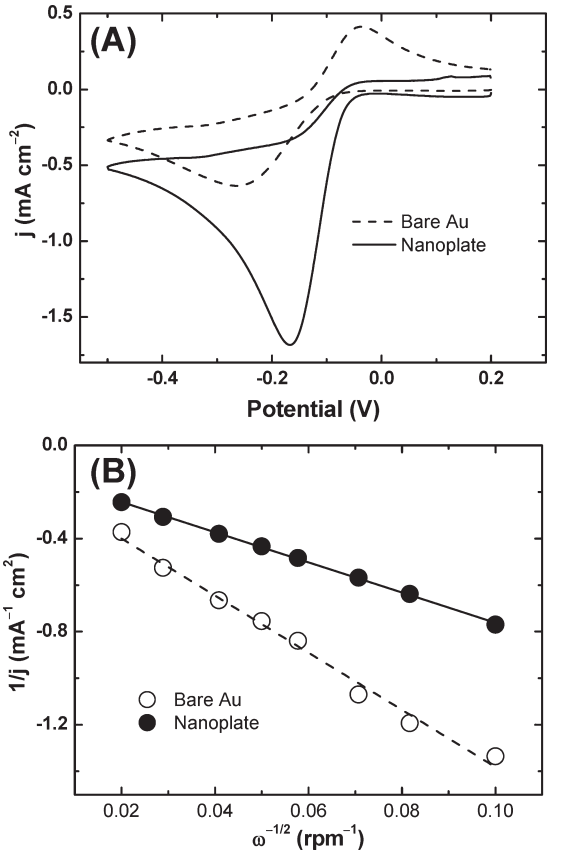

Figure 4. (A) Cyclic voltammograms obtained on bare and nanoplate Au surfaces in 0.1 M NaOH. Scan rate: 50 mV/s. (B) Koutecky−Levich plots obtained from RDE measurements on bare (−0.3 V) and nanoplate Au (−0.2 V) surfaces in 0.1 M NaOH. Scan rate: 10 mV/s.

nanoplate Au structures electrocatalytically active for oxygen reduction in basic media via a direct four-electron reduction mechanism. It has been reported that AuNPs enriched in the Au(100) and Au(110) facets can be electrochemically deposited on glassy carbon electrode surfaces in the presence of cysteine as an additive,[30] which accomplish a 4-electron reduction of oxygen to water in basic media.[31]

Since the electrooxidation of glucose is sensitive to the surface orientation of Au electrodes,[32,33] it would be informative to correlate the electrocatalytic activity of the Au nanoplate toward glucose oxidation with its electrocatalytic activity. Presented in Figure 5 is the electrooxidation of glucose, where a significant increase in the anodic current is measured on a nanoplate Au surface compared to a bare Au surface. The extent of increase in the anodic current for glucose oxidation at nanoplate Au surfaces is larger than that expected from the increase in the ESA, which indicates that the nanoplate Au surfaces are electrocatalytically active for glucose oxidation. Although there is one anodic peak at 0.35 V on bare Au surfaces, two anodic peaks are observed on nanoplate Au surfaces. The anodic peak at 0.25 V, which is ca. 0.1 V negatively shifted compared to that observed on bare Au surfaces, is known to be usually observed for glucose oxidation on nanostructured Au surfaces.[34,35] This may be partly ascribed to the presence of steps and kinks on Au surfaces, as evidenced by the XRD data. Another anodic peak is observed on nanoplate Au surfaces at around 0.0 V, which is not found on bare Au surfaces. This anodic wave for glucose electrooxidation has been previously

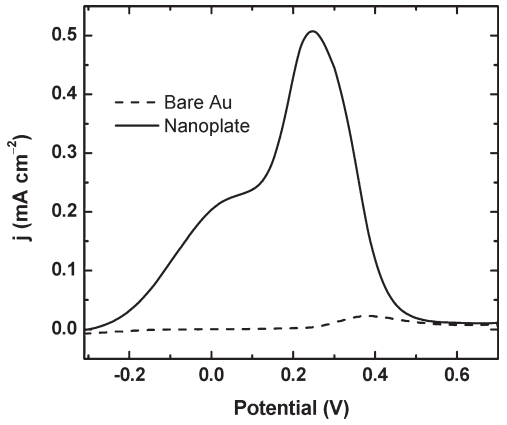

Figure 5. Anodic scans obtained on bare and nanoplate Au surfaces in 10 mM glucose +0.1 M phosphate buffer (pH 7.0). Scan rate: 10 mV/s.

reported to be observed on Au(110) single-crystal surfaces[33,36] or on Au nanostructures retaining Au(110) facets,[34,35] indicative of the presence of Au(110) facets on the nanoplate Au surfaces.

The unique catalytic activity of nanoplate Au surfaces toward the electrooxidation of glucose appears conspicuous in the presence of Cl^-, which is a well-known species deactivating the electrocatalytic activity for glucose oxidation.[36] Compared to other nanostructured Au structures electrodeposited at −0.9 and −1.0 V, exhibiting similar electrocatalytic activities for glucose oxidation, the well-defined nanoplate Au surfaces maintain relatively higher electrocatalytic activity in the presence of Cl^- (see Figure S9 in the Supporting Information). The anodic current level of a nanoplate Au surface for glucose oxidation in the presence of 10 mM of Cl^- is ca. 70% of that measured in the absence of Cl^-, which is a fairly higher level compared to bare Au surfaces or other Au nanostructures.[35] The sustained electrocatalytic activity of nanoplate Au in the presence of Cl^- would be useful in glucose detection in Cl^--rich biological environments, and the application of nanoplate surface structures on the development of practical glucose sensors is underway.

CONCLUSIONS

Au nanoplate structures can be fabricated by a simple electrodeposition process from a Au(I) cyanide complex in the absence of additives or premodification of electrode surfaces. The nanoplate Au structures electrodeposited from $Au(CN)_2^-$ are unique in shape compared to other Au nanostructures electrodeposited from $AuCl_4^-$ previously reported, which can be ascribed to the unique mechanism for electrodeposition of $Au(CN)_2^-$ at low overpotential regions. In contrast to other electrodeposited Au nanostructures, those reported here are rich in Au(110) and Au(100) domains, which exhibit electrocatalytic activities for oxygen reduction and glucose oxidation. Straightforward preparation of well-defined nanoplate Au structures will provide new opportunities for the utilization of Au-based substrates in other electroanalytical applications through further chemical modification of Au surfaces.

ASSOCIATED CONTENT

Supporting Information. Additional SEM images, XRD spectrum, and cyclic voltammograms (PDF). This material is available free of charge via the Internet at http://pubs.acs.org

AUTHOR INFORMATION

Corresponding Author
*E-mail: jongwonkim@chungbuk.ac.kr.

ACKNOWLEDGMENT

This research was financially supported by the Ministry of Education, Science Technology (MEST) and Korea Institute for Advancement of Technology (KIAT) through the Human Resource Training Project for Regional Innovation. This work was supported by the grant of the Korean Ministry of Education, Science and Technology (The Regional Core Research Program/Chungbuk BIT Research-Oriented University Consortium).

REFERENCES

(1) Daniel, M. C.; Astruc, D. *Chem. Rev.* **2004**, *104*, 293–346.
(2) Hicks, J. F.; Seok-Shon, Y.; Murray, R. W. *Langmuir* **2002**, *18*, 2288–2294.
(3) Abdelrahman, A. I.; Mohammad, A. M.; Okajima, T.; Ohsaka, T. *J. Phys. Chem. B* **2006**, *110*, 2798–2803.
(4) El-Deab, M. S.; Ohsaka, T. *Electrochem. Commun.* **2002**, *4*, 288–292.
(5) El-Deab, M. S.; Sotomura, T.; Ohsaka, T. *J. Electrochem. Soc.* **2005**, *152*, C730–C737.
(6) Plowman, B.; Ippolito, S. J.; Bansal, V.; Sabri, Y. M.; O'Mullane, A. P.; Bhargava, S. K. *Chem. Commun.* **2009**, 5039–5041.
(7) Tian, Y.; Liu, H. Q.; Zhao, G. H.; Tatsuma, T. *J. Phys. Chem. B* **2006**, *110*, 23478–23481.
(8) Guo, S.; Wang, L.; Wang, E. *Chem. Commun.* **2007**, 3163–3165.
(9) Zhang, H.; Xu, J. J.; Chen, H. Y. *J. Phys. Chem. C* **2008**, *112*, 13886–13892.
(10) Wang, L.; Guo, S. J.; Hu, X. G.; Dong, S. J. *Electrochem. Commun.* **2008**, *10*, 95–99.
(11) Zeng, J.; Ma, Y. Y.; Jeong, U.; Xia, Y. N. *J. Mater. Chem.* **2010**, *20*, 2290–2301.
(12) Wilkinson, P. *Gold Bull.* **1986**, *19*, 75–81.
(13) Green, T. A. *Gold Bull.* **2007**, *40*, 105–114.
(14) Umar, A. A.; Oyama, M. *Cryst. Growth Des.* **2006**, *6*, 818–821.
(15) Umar, A. A.; Oyama, M.; Salleh, M. M.; Majlis, B. Y. *Cryst. Growth Des.* **2009**, *9*, 2835–2840.
(16) Martín, H.; Carro, P.; Hernández Creus, A.; González, S.; Salvarezza, R. C.; Arvia, A. J. *Langmuir* **1997**, *13*, 100–110.
(17) Trasatti, S.; Petrii, O. A. *Pure Appl. Chem.* **1991**, *63*, 711–734.
(18) Hamelin, A. *J. Electroanal. Chem.* **1996**, *407*, 1–11.
(19) Hamelin, A. *J. Electroanal. Chem.* **1984**, *165*, 167–180.
(20) Hernandez, J.; Solla-Gullon, J.; Herrero, E. *J. Electroanal. Chem.* **2004**, *574*, 185–196.
(21) Hernandez, J.; Solla-Gullon, J.; Herrero, E.; Aldaz, A.; Feliu, J. M. *J. Phys. Chem. C* **2007**, *111*, 14078–14083.
(22) Chen, Y.; Schuhmann, W.; Hassel, A. W. *Electrochem. Commun.* **2009**, *11*, 2036–2039.
(23) Soleimany, L.; Dolati, A.; Ghorbani, M. *J. Electroanal. Chem.* **2010**, *645*, 28–34.
(24) Bozzini, B.; Mele, C.; Romanello, V. *J. Electroanal. Chem.* **2006**, *592*, 25–30.
(25) Sawaguchi, T.; Yamada, T.; Okinaka, Y.; Itaya, K. *J. Phys. Chem.* **1995**, *99*, 14149–14155.
(26) Liu, J.; Duan, J. L.; Toimil-Molares, E.; Karim, S.; Cornelius, T. W.; Dobrev, D.; Yao, H. J.; Sun, Y. M.; Hou, M. D.; Mo, D.; Wang, Z. G.; Neumann, R. *Nanotechnology* **2006**, *17*, 1922–1926.
(27) Ha, T. H.; Koo, H. J.; Chung, B. H. *J. Phys. Chem. C* **2007**, *111*, 1123–1130.
(28) Xiong, Y. J.; McLellan, J. M.; Chen, J. Y.; Yin, Y. D.; Li, Z. Y.; Xia, Y. N. *J. Am. Chem. Soc.* **2005**, *127*, 17118–17127.

(29) Markovic, N. M.; Adzic, R. R.; Vesovic, V. B. *J. Electroanal. Chem.* **1984**, *165*, 121–133.
(30) El-Deab, M. S.; Sotomura, T.; Ohsaka, T. *J. Electrochem. Soc.* **2005**, *152*, C1–C6.
(31) El-Deab, M. S.; Sotomura, T.; Ohsaka, T. *Electrochem. Commun.* **2005**, *7*, 29–34.
(32) Adzic, R. R.; Hsiao, M. W.; Yeager, E. B. *J. Electroanal. Chem.* **1989**, *260*, 475–485.
(33) Hsiao, M. W.; Adzic, R. R.; Yeager, E. B. *J. Electrochem. Soc.* **1996**, *143*, 759–767.
(34) Seo, B.; Kim, J. *Electroanalysis* **2010**, *22*, 939–945.
(35) Cho, S.; Shin, H.; Kang, C. *Electrochim. Acta* **2006**, *51*, 3781–3786.
(36) Hsiao, M. W.; Adzic, R. R.; Yeager, E. B. *Electrochim. Acta* **1992**, *37*, 357–363.